Supplementary Information

Chemically-informed active learning enables data-efficient multi-objective optimization of self-healing polyurethanes

Kang Liang†, Xinke Qi†, Xu Xiao, Li Wang, and Jinglai Zhang**

† K. Liang and X. Qi contributed equally to this work

K. Liang, X. Qi, X. Xiao, L. Wang, J. Zhang

Henan Key Laboratory of Protection and Safety Energy Storage of Light Metal Materials

College of Chemistry and Molecular Sciences

Henan University

Kaifeng, Henan 475004, P. R. China

*Corresponding authors: L. Wang, chemwangl@henu.edu.cn; J. Zhang, zhangjinglai@henu.edu.cn

Supplementary Text

Materials

Polytetramethylene ether glycol (PTMEG M_n = 1000 g mol^{-1}), 4,4'-biphenol (BP), 2,6-pyridinedimethanol (PDM), 4-bromo-1,8-naphthalic anhydride, 2-amino-1,3-propanediol and *N*-acetyl ethylenediamine were purchased from Aladdin. Isophorone diisocyanate (IPDI), dibutyltin dilaurate (DBTDL), bis(2-hydroxyethyl) disulfide (HEDS) and 4,4′-dicyclohexylmethane diisocyanate (HMDI) were obtained from Macklin. Anhydrous *N,N*-dimethylformamide (DMF) and *N,N*-dimethylacetamide (DMAc) were purchased from Adamas. All chemicals were used without further purification.

Characterization

The chemical structures of the polymers were analyzed using Fourier transform infrared spectroscopy (FT-IR, Bruker, VERTEX 80v) and proton nuclear magnetic resonance spectroscopy (^{1}H NMR, Bruker, AVANCE NEO 400M). The fluorescence emission spectra were captured using a HORIBA FluoroMax+ spectrofluorometer equipped with a fiber-coupled diode laser excitation. The microphase separation structure of samples was examined using atomic force microscopy (AFM, Bruker, Dimension Icon) in tapping mode. The corrosion behavior of samples in 3.5 wt% NaCl solution was studied by potentiodynamic polarization (PDP) curves and electrochemical impedance spectroscopy (EIS) through an electrochemical workstation (CH Instruments CHI660E). Electrochemical tests were performed with a three-electrode system including a coated or uncoated bare Q235 steel sample as the working

electrode (exposed surface area of 1 cm^2), a saturated calomel electrode as the reference electrode and a platinum electrode as the counter electrode. PDP curves were measured from -2000 to -1000 mV at a scan rate of 1mV s^{-1}. The EIS measurements were carried out over a frequency range of 10^5 to 10^{-2} Hz with a sinusoidal perturbation of 5 mV. For the salt spray test, the P20B-coated samples were placed in a spray machine (chamber temperature at 35 °C) and exposed to a continuous salt spray with a 5.0 wt% NaCl solution.

Mechanical and self-healing tests

Mechanical tensile tests were conducted on a universal tensile machine (Shenzhen SUNS UTM4203) with a tensile rate of 50 mm min^{-1}. Each measurement was repeated at least three times. The toughness was calculated by integrating the area under the stress-strain curves.

For the self-healing test, the samples were cut into two pieces and the cut sample strips were brought into contact and allowed to self-heal under specific conditions. Then the tensile test was conducted by the universal tensile machine following the aforementioned procedure. Each measurement was repeated at least three times. The self-healing efficiency (η_σ, η_ε and η_T) can be defined by the following formula:

$$\eta_\sigma = \frac{\sigma_{healed}}{\sigma_{original}} \quad (1)$$

$$\eta_\varepsilon = \frac{\varepsilon_{healed}}{\varepsilon_{original}} \quad (2)$$

$$\eta_T = \frac{T_{healed}}{T_{original}} \quad (3)$$

where σ_{healed} and $\sigma_{original}$ are the tensile strengths of the healed and pristine samples, respectively. ε_{healed} and $\varepsilon_{original}$ denote the elongation at break for the healed and original specimens, respectively. T_{healed} and $T_{original}$ represent the toughness of the healed and the original samples, respectively. When the mechanical property value of the healed specimen exceeds that of the original sample, the self-healing efficiency is calculated as 100.0%.

The relative error between predicted and experimental values is calculated as follows:

$$\text{relative error} = \left| \frac{y_{exp} - y_{pred}}{y_{exp}} \right| \times 100\% \quad (4)$$

where y_{pred} and y_{exp} are the predicted and experimental values, respectively. For mechanical property indicators, logarithmic values of both predicted and experimental data are adopted in the relative error calculation.

Machine learning details

All modeling activities were performed in Python (version 3.8.18), using libraries including Pandas 1.5.3 and NumPy 1.24.3 for data analysis, scikit-learn 1.2.0 for performing GBR algorithm and model analysis, Pymoo 0.6.1.2 for implementing the NSGA-III algorithm.

Gradient Boosting Regression algorithm

The specific process of Gradient Boosting Regression (GBR) algorithm is as follows. Given a training dataset $D = \{x_i, y_i\}_{i=1}^{N}$, the goal of gradient boosting is to find an

approximation, $F(x)$, of the function $F_0(x)$, which maps instances x to their output values y, by minimizing the expected value of a given loss function, $L(y,F(x))$. Gradient boosting builds an additive approximation of $F(x)$ as a weighted sum of functions:

$$F(x) = \sum_{m=1}^{M} \rho_m h_m(x) \tag{5}$$

Where ρ_m is the weight of the m-th function, $h_m(x)$. These functions are the models of the ensemble (e.g., decision trees). The approximation is constructed iteratively. First, a constant approximation of $F_0(x)$ is obtained as:

$$F_0(x) = argmin_{\alpha} \sum_{i=1}^{N} L(y_i, \alpha) \tag{6}$$

Subsequent models are expected to minimize:

$$F_m(x) = F_{m-1}(x) + \rho_m h_m(x) \tag{7}$$

$$(\rho_m, h_m(x)) = argmin_{\rho,h} \sum_{i=1}^{N} L(y_i, F_{m-1}(x_i) + \rho h(x_i)) \tag{8}$$

However, instead of solving the optimization problem directly, each h_m can be seen as a greedy step in a gradient descent optimization for F. For that, each model h_m is trained on a new dataset $D = \{x_i, r_{mi}\}_{i=1}^{N}$, where the pseudo-residuals r_{mi} are calculated by:

$$r_{mi} = -\left[\frac{\partial L(y_i, F(x_i))}{\partial F(x_i)} \right]_{F(x_i)=F_{m-1}(x_i)} \tag{9}$$

The value of ρ_m is subsequently computed by solving a line search optimization problem.

During the training process, the dataset was divided, with 80% allocated for training and 20% for testing. Since the value ranges of these variables differ significantly, which may pose challenges for model training, we addressed this issue by applying the standardization formula:

$$x_{\text{std}} = \frac{x - \mu}{\sigma} \tag{10}$$

This transformation standardizes the different component variables to have a mean (μ) of 0 and a standard deviation (σ) of 1. Additionally, due to the mechanical property values spanning 2-3 orders of magnitude, we utilized the logarithms of these properties. After standardizing all feature values, three mechanical properties (σ, ε, T) and corresponding self-healing efficiency (η_σ, η_ε, η_T) were set as the prediction targets. To optimize the model's performance, the grid search method was employed to tune the hyperparameters and select the optimal parameter combination. The search ranges for the GBR algorithm's hyperparameters are shown in Table S17.

Model metrics

The accuracy of the models is assessed using Mean Absolute Error (*MAE*) and the Coefficient of Determination (R^2), defined as follows:

$$MAE = \frac{1}{n}\sum_{i=1}^{n}\left|y_i - \hat{y}_i\right| \tag{11}$$

$$R^2 = 1 - \frac{\sum_{i=1}^{n}(y_i - \hat{y}_i)^2}{\sum_{i=1}^{n}(y_i - \overline{y})^2} \tag{12}$$

where y_i represent the experimental values, $\hat{y}_i$ are the corresponding predicted values, with $\overline{y}_i$ being the average of the experimental values. A smaller MAE and an R^2 value closer to 1 indicate a better-performing ML model.

Leave-one-out cross-validation

We employed leave-one-out cross-validation to evaluate the reliability of the MD-9A, MD-15, MD-20, and MD-25 models (the hyperparameters for each model remained). In this approach, each data point is iteratively used as the validation set, while the remaining data points are used for model training. This process is repeated until every data point has served as the validation set once. The predictive performance of each model is quantified by the average value of the mean absolute error (*MAE*) across all iterations, enabling a direct comparison of model accuracy.

Multi-objective optimization

The Non-dominated Sorting Genetic Algorithm (NSGA) was a genetic algorithm based on Pareto dominance and non-dominated sorting, originally proposed by Srinivas and Deb in the early 1990s.[1] In 2002, Deb introduced an improved version, NSGA-II, which incorporated fast non-dominated sorting and elitism to significantly enhance optimization efficiency and computational speed.[2] However, as the number of objective functions increases, NSGA-II can face difficulties in maintaining population diversity and effectively handling high-dimensional Pareto fronts.To overcome these limitations, NSGA-III was proposed by Kalyanmoy Deb and colleagues in 2014.[3] This algorithm introduced a reference-point-based non-dominated sorting method, specifically designed for high-dimensional multi-objective optimization problems. Given that this study involves six optimization objectives, NSGA-III was selected as the preferred optimization framework.

In this work, the NSGA-III genetic algorithm combined with the GBR models was employed to simultaneously optimize the mechanical (σ, ε and T) and self-healing (η_σ, η_ε and η_T) indicators. The aim was to maximize the values of the six objectives while maintaining high predictive accuracy. The primary process of the NSGA-III algorithm was shown in Fig. S22. The initial hyperparameters of the NSGA-III multi-objective optimization algorithm were as follows: an initial population of 500, a maximum number of generations of 500, a crossover probability of 0.8, and a crossover distribution index of 20. When employing NSGA-III for the optimization of six objectives, the optimization range for the elements was set as follows: the proportion of PTMEG from 0.2 to 0.4, the proportion of IPDI from 0.3 to 0.7, the proportion of HEDS from 0 to 0.5, and the proportion of NIAM from 0 to 0.5. Subsequently, an initial population of 500 individuals (i.e., 500 PU compositions) was generated within this range, and 1000 offspring were obtained through population crossover and mutation. The selected models (GBR) were used to predict σ, ε, T, η_σ, η_ε and η_T. After non-dominated sorting of the six attributes, 500 individuals on the Pareto front were selected for the next iteration. The optimization terminated and results were outputed once the number of iterations reached 500 or the termination criteria were met.

To better assess the comprehensive performance of PSSNM, three mechanical properties indicators (σ, ε, and T) and corresponding self-healing capabilities are transformed into a comparative single value, referred to as the comprehensive objective. To mitigate the impact of order-of-magnitude differences among the six objectives, the

values of all six targets were normalized to the interval [0,1] through data normalization. The calculation formula is as follows:

$$X_{\text{norm}} = \frac{X_{\max} - X_{\min}}{X - X_{\min}} \tag{13}$$

where $X_{\min}$ and $X_{\max}$ are the minimum and maximum values in the dataset, respectively. After numerical mapping of the six objectives, the comprehensive index (Z) can be calculated using a weighted method. In this way, mechanical properties indicators and self-healing capabilities were transformed into a comprehensive mechanical performance index ($Z1$) and a self-healing performance index ($Z2$) (Detailed methodologies are provided in the main text).

The process of the NSGA-III algorithm (Fig. S22) used in this study is as follows:

(1) Initialization: An initial population of 500 individuals is randomly generated within the specified ranges for the components (PTMEG: 0.2-0.4, IPDI: 0.3-0.7, HEDS: 0-0.5, NIAM: 0-0.5). Each individual represents a potential solution to the problem, characterized by a set of decision variables.

(2) Selection, crossover, and mutation: New offspring are produced by selecting and mating outstanding individuals through crossover (with a probability of 0.8 and a distribution index of 20) and mutation operations. This generates a total of 1000 offspring.

(3) Fast non-dominated sorting: The combined parent and offspring populations undergo non-dominated sorting, categorizing individuals into different levels based on their dominance relationships.

(4) Calculation crowding distance: Crowding distance is calculated to measure the density of individuals in the objective function space. This helps maintain population diversity by favoring individuals in less crowded regions.

(5) Selection of individuals: The next generation population is selected from the current population based on non-dominated sorting and crowding distance. This ensures a balance between convergence and diversity.

(6) Iteration: The algorithm checks whether the termination conditions are met. These conditions include reaching the maximum number of iterations (500) or achieving convergence criteria. If the termination conditions are not met, the process returns to step 2.

By following this process, the NSGA-III algorithm effectively optimizes the six objectives, generating a Pareto front that represents the trade-offs between mechanical properties and self-healing capabilities. The GBR models are used to predict the performance of different PU compositions, and the comprehensive indices ($Z1$ and $Z2$) allow for a more holistic evaluation of the materials' performance.

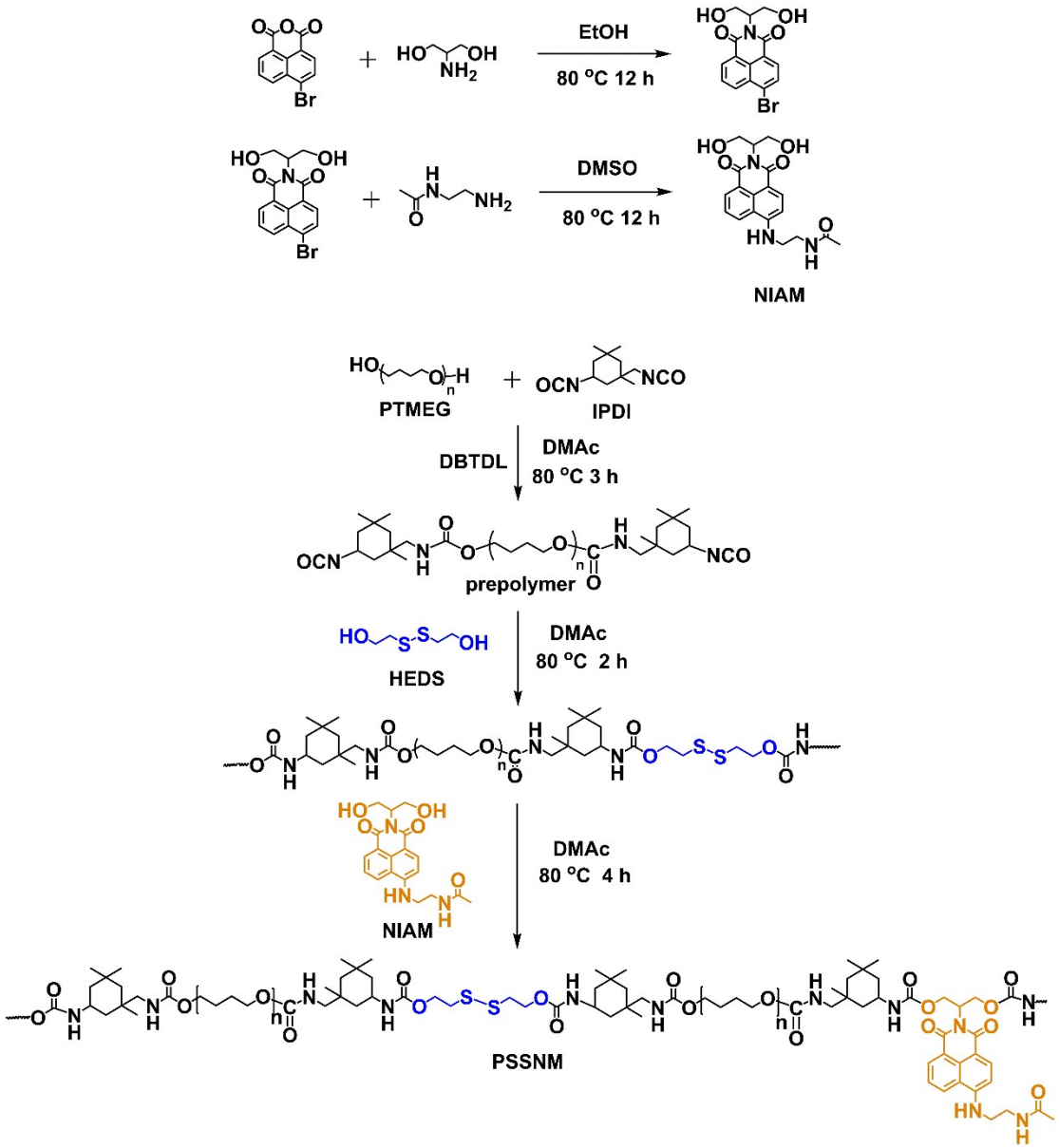

Fig. S1. Synthesis routes of NIAM and PSSNM.

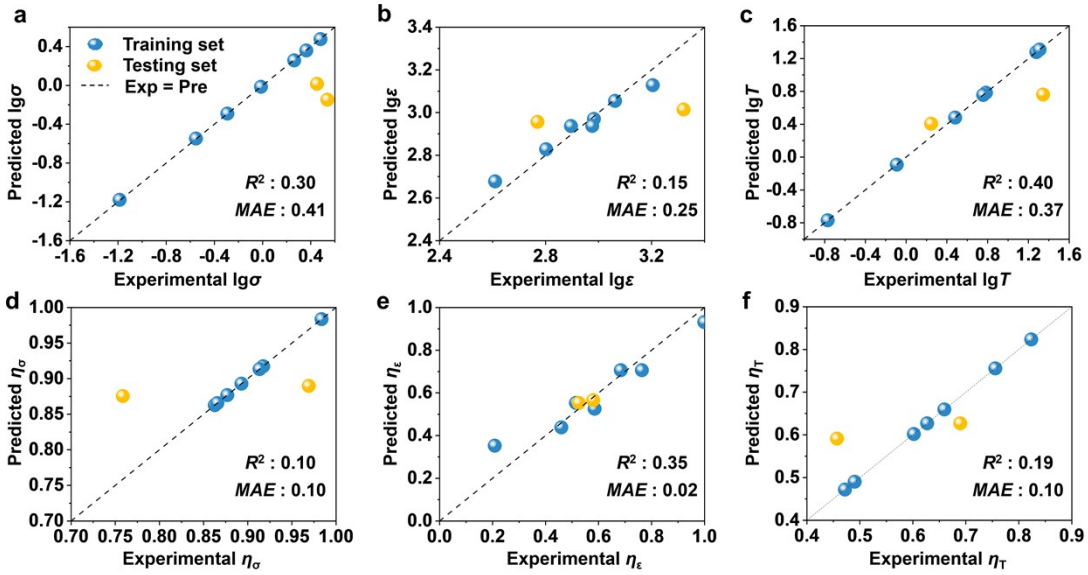

Fig. S2. Comparative predictions of properties on training and testing data using GBR model (MR-9). Experimental versus predicted results: (a) for lgσ, (b) for lgε, (c) for lg$T$, (d) for η_σ, (e) for η_ε, (f) for η_T.

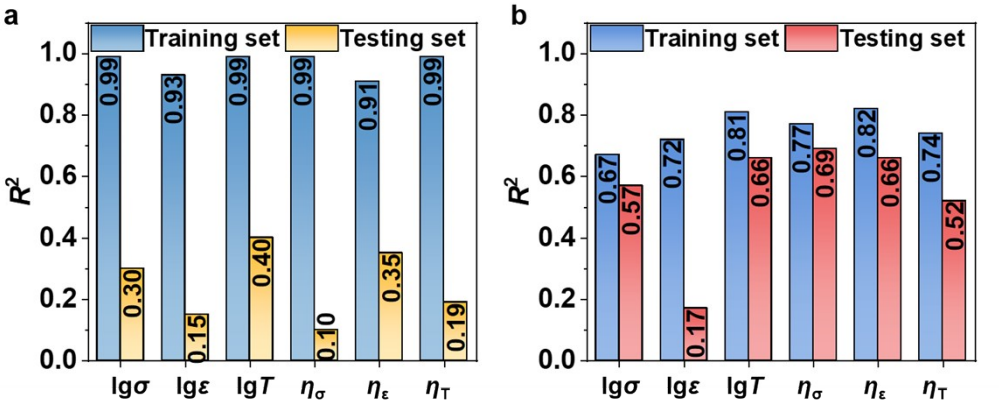

Fig. S3. Single-objective model establishment. (a) R^2 values of MR-9, (b) R^2 values of MR-12.

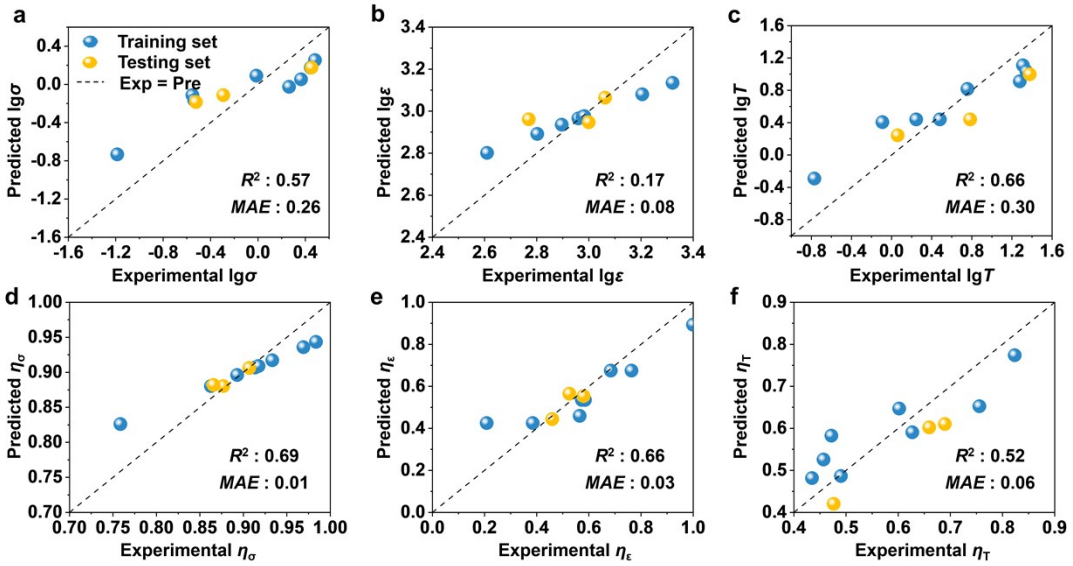

Fig. S4. Comparative predictions of properties on training and testing data using GBR model (MR-12). Experimental versus predicted results: (a) for lgσ, (b) for lgε, (c) for lg$T$, (d) for η_{σ}, (e) for η_{ε}, (f) for η_{T}.

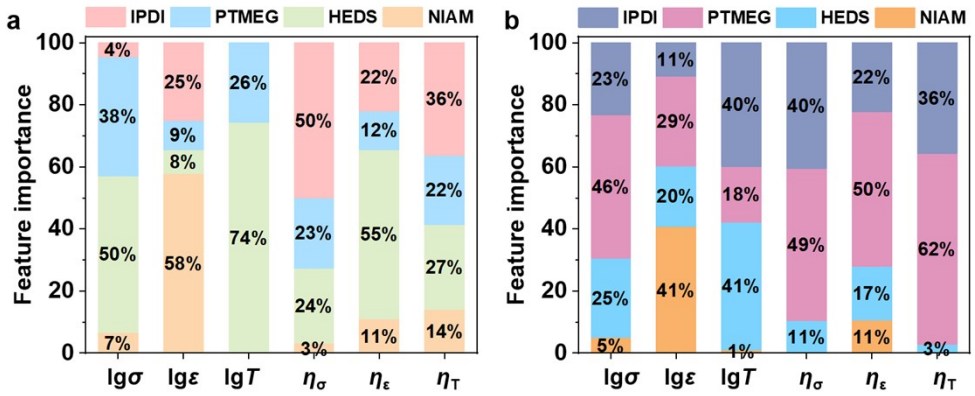

Fig. S5. Feature importance analysis of MR-9 and MR-12 models. Feature importance of PSSNM compositions on each of performance metrics as determined by GBR analysis: (a) MR-9, (b) MR-12.

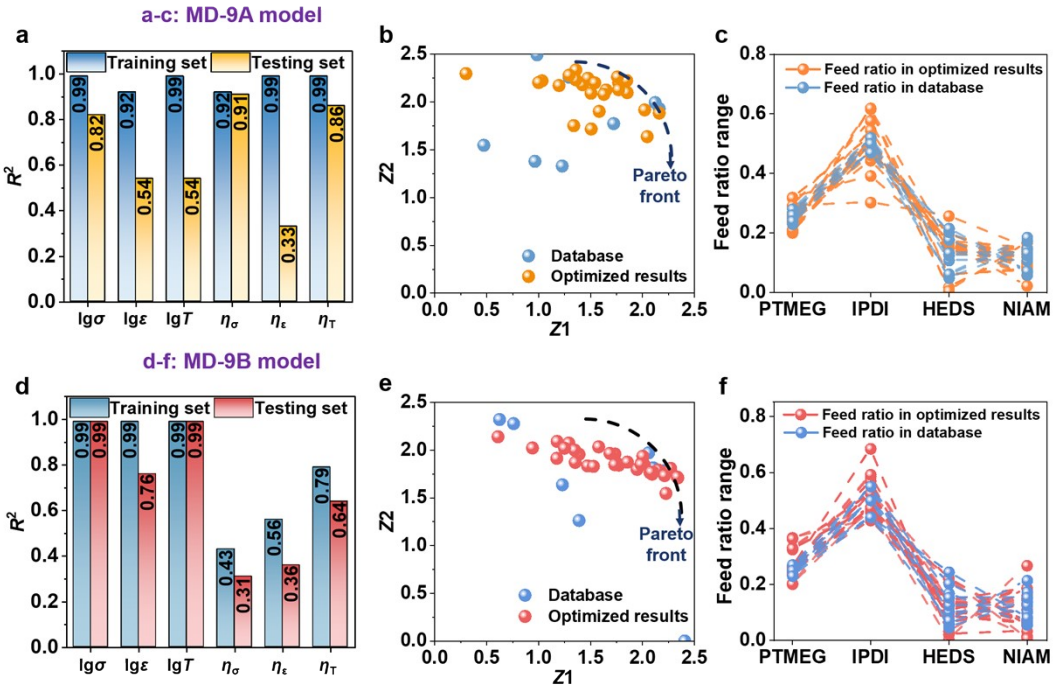

Fig. S6. Accuracy and multi-objective optimization results of MD-9A and MD-9B models. Single-objective model establishment: (a) R^2 values of MD-9A, (d) R^2 values of MD-9B. The comprehensive performance index of mechanical and self-healing properties within the dataset, along with the Pareto front based on (b) MD-9A, (e) MD-9B. Feed ratio of PSSNM within the dataset, together with the Pareto front based on (c) MD-9A, (f) MD-9B.

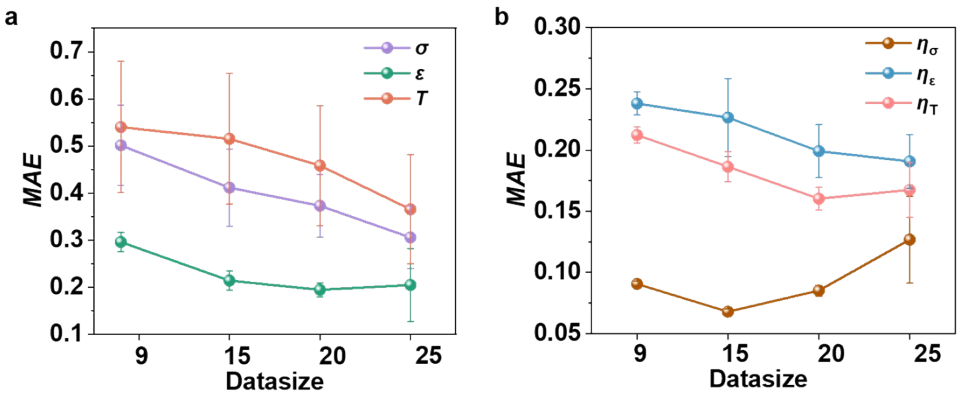

Fig. S7. Leave-one-out cross-validation results comparing model prediction accuracy across datasets of different sizes (MD-9A, MD-15, MD-20, MD-25). (a) The average value of *MAE* values for the prediction of σ, ε, and T. (b) The average value of *MAE* values for their corresponding self-healing performance indicators (η_σ, η_ε, *and* η_T).

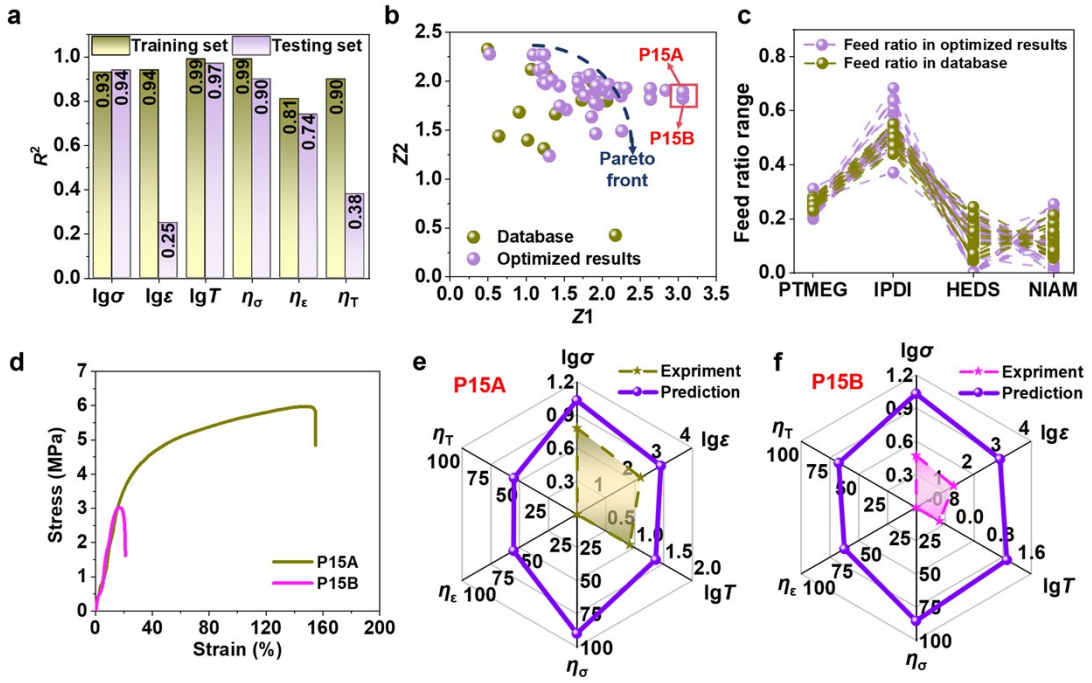

Fig. S8. Multi-objective optimization and experimental verification results of MD-15 model. (a) Single-objective model establishment: R^2 values of MD-15. (b) The comprehensive performance index of mechanical and self-healing properties within the dataset, along with the Pareto front based on MD-15. (c) Feed ratio of PSSNM within the dataset, together with the Pareto front based on MD-15. (d) Stress-strain curves of P15A and P15B. Comparison of predicted and experimental results of (e) P15A and (f) P15B.

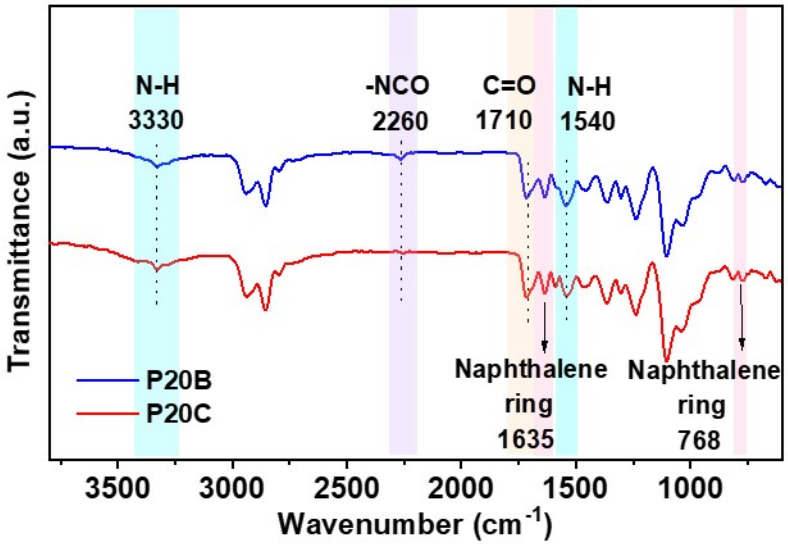

Fig. S9. FT-IR spectra of P20B and P20C.

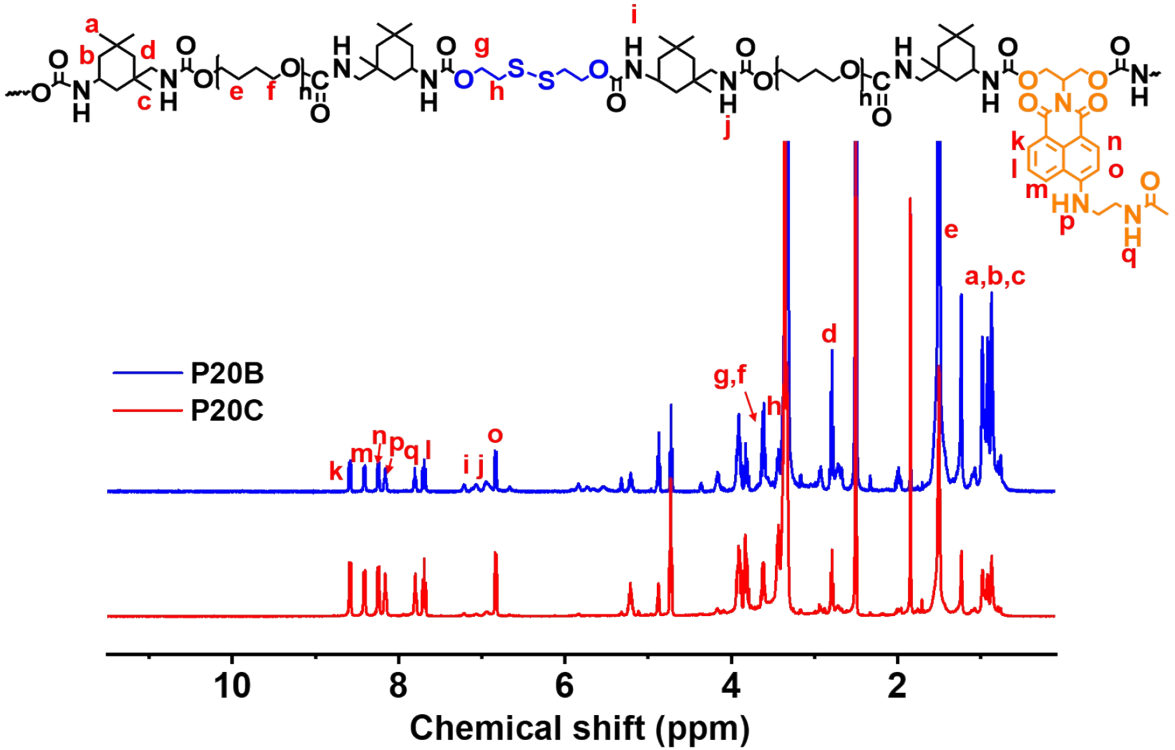

Fig. S10. ^{1}H NMR spectra of P20B and P20C.

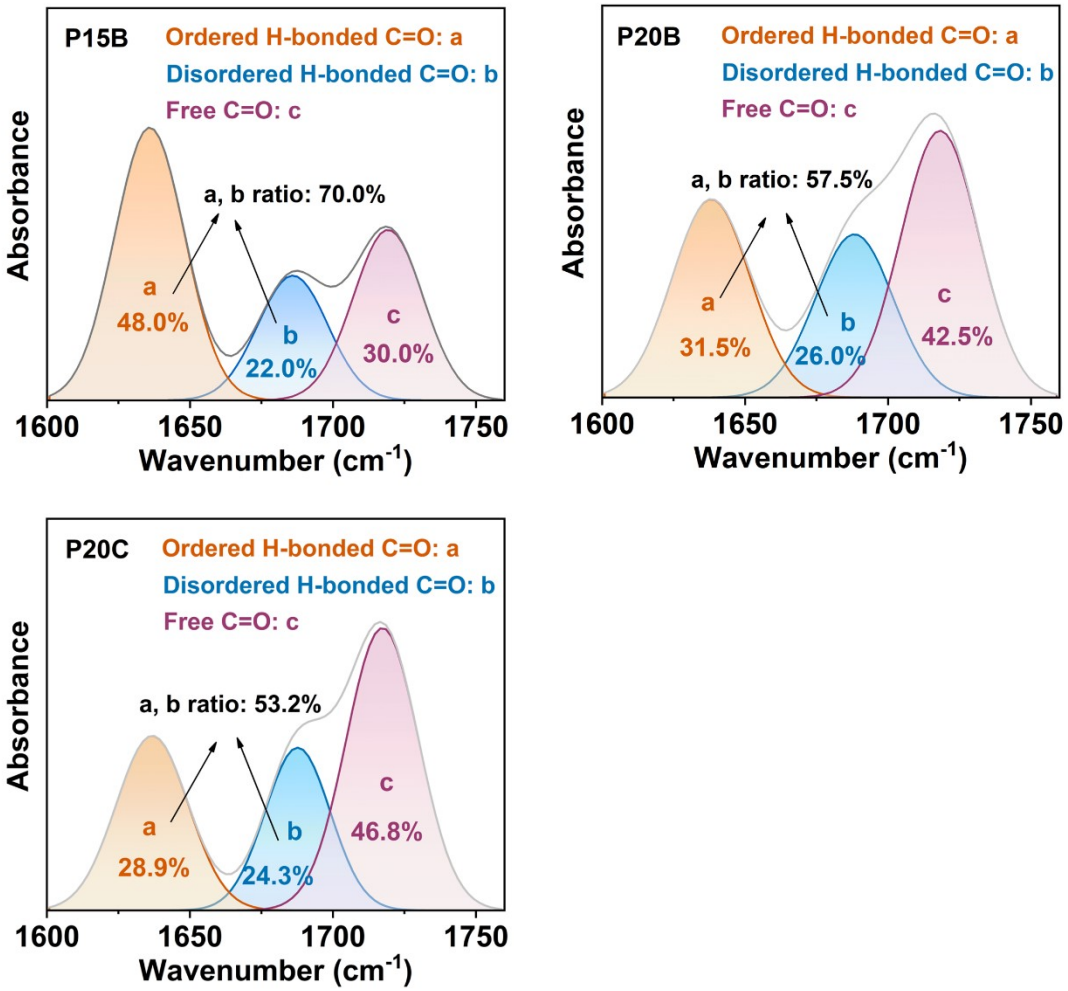

Fig. S11. FT-IR spectra of P15B, P20B and P20C in the C=O stretching vibration region.

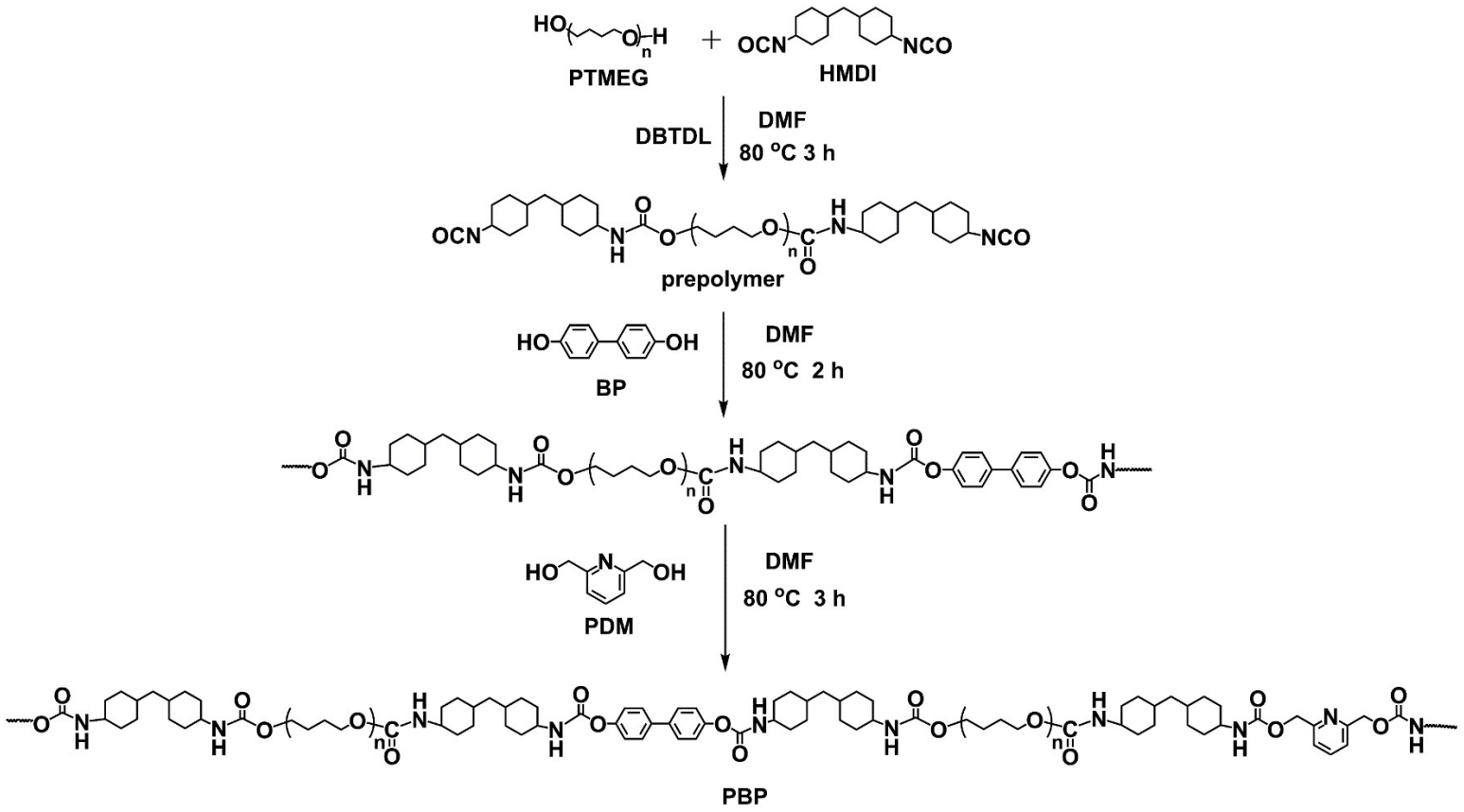

Fig. S12. Synthesis route of PBP.

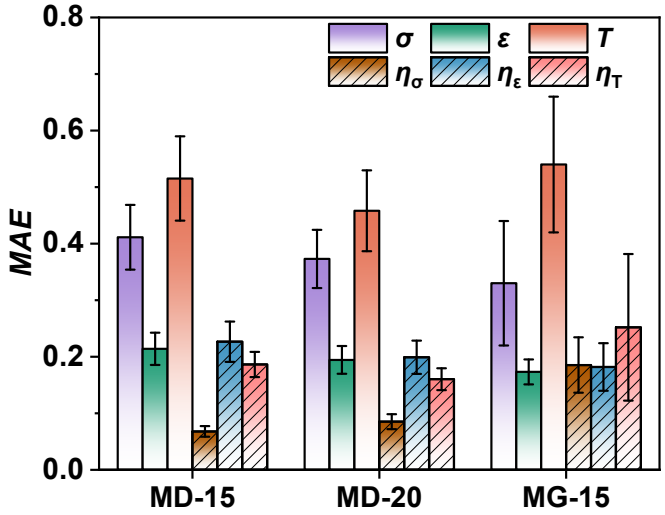

Fig. S13. Leave-one-out cross-validation results. Comparing model prediction accuracy across datasets of different sizes (MD-15, MD-20, MG-15).

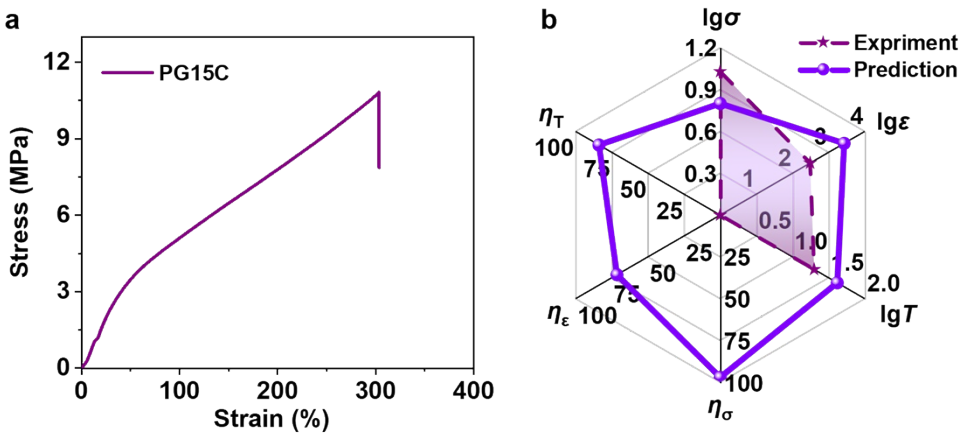

Fig. S14. Experimental verification results of PG15C. (a) Stress-strain curve of the PG15C. (b) Comparison of predicted and experimental results of PG15C.

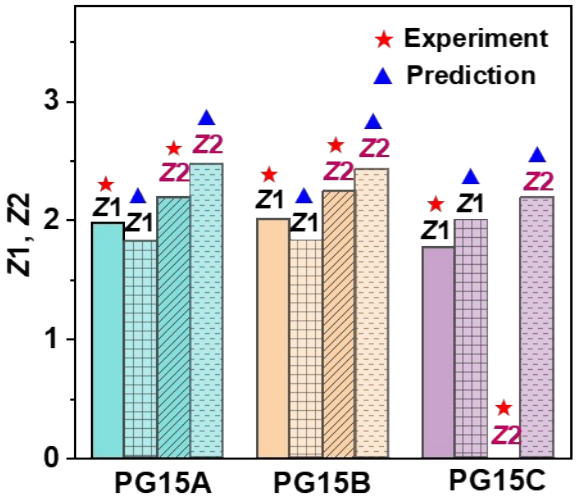

Fig. S15. Comprehensive performance indicators of PG15A, PG15B and PG15C.

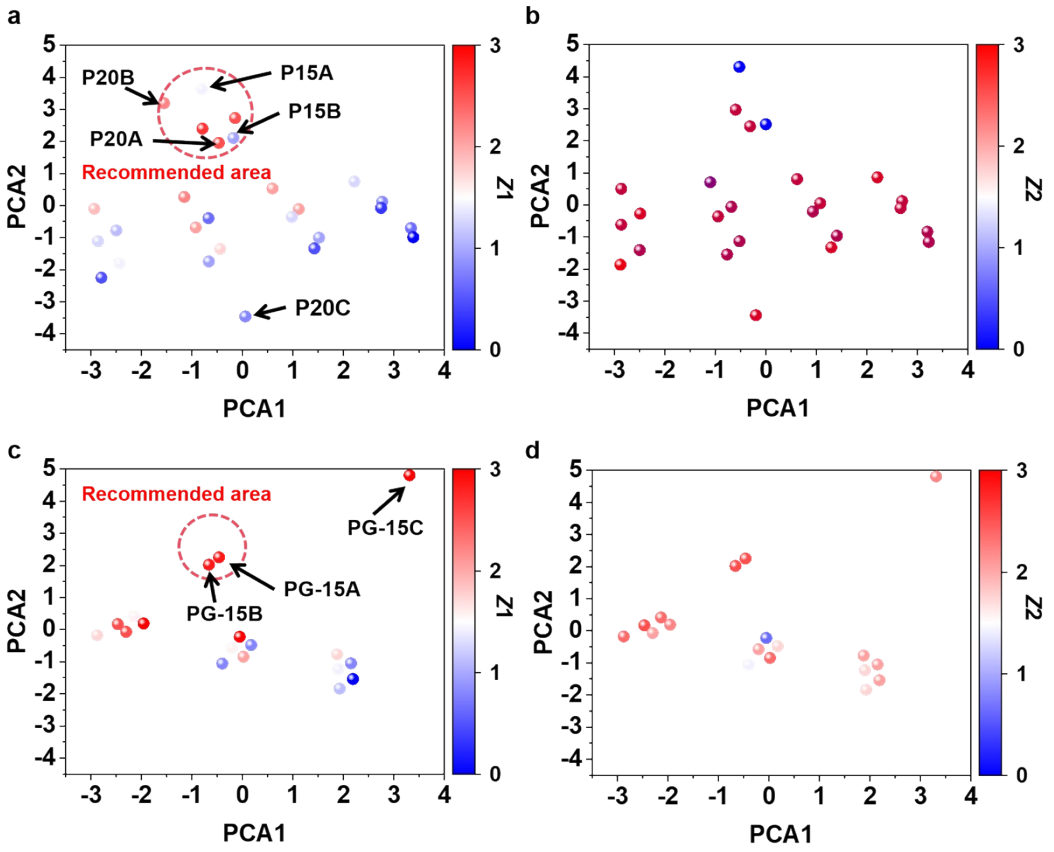

Fig. S16. The component distribution maps after PCA dimensionality reduction. (a) and (b) show the distribution of MD-25 database samples in principal component space. (c) and (d) show the distribution of MR-15 database samples in principal component space (Color gradients represent the changes in *Z*1 and *Z*2 scores).

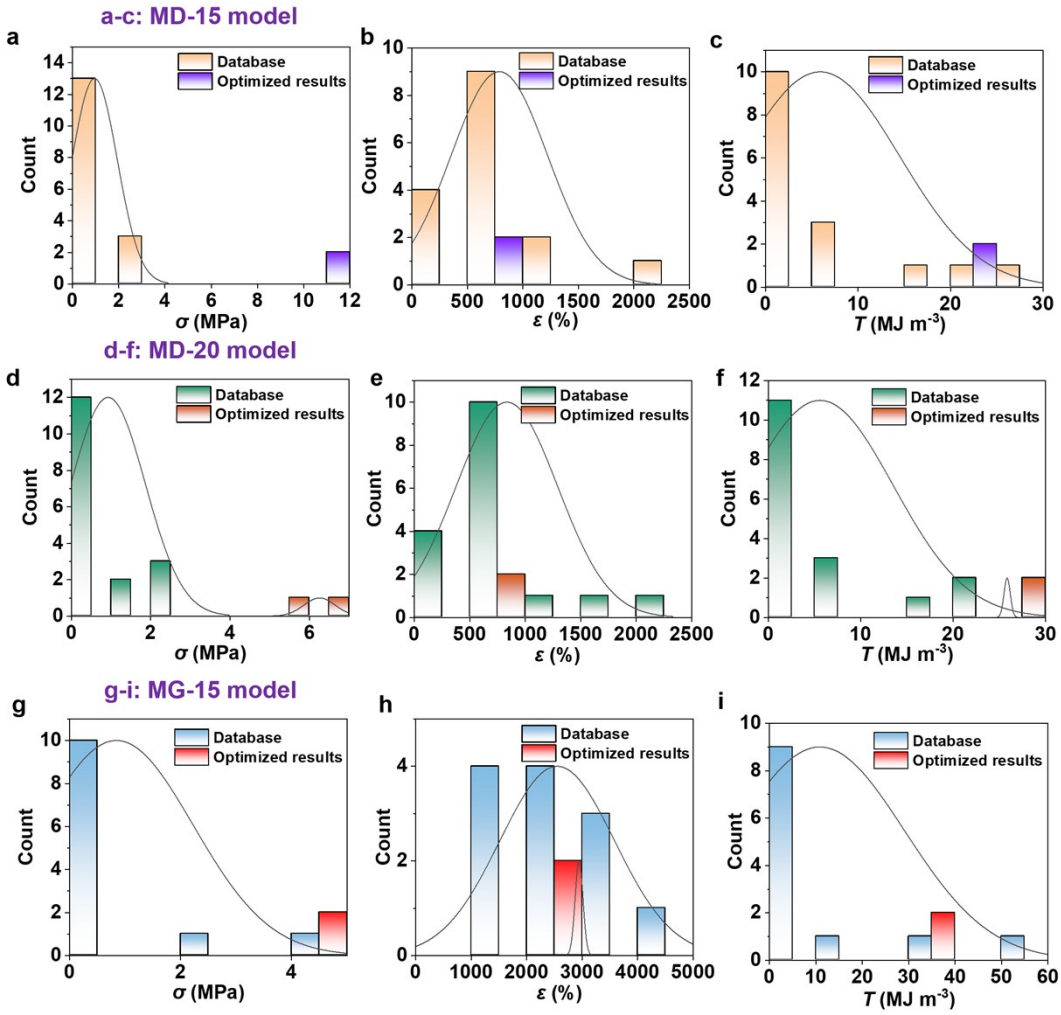

Fig. S17. Analysis of mechanical properties distribution. Mechanical properties distribution of the original database and the corresponding model recommendations from (a-c) MD-15, (d-f) MD-20, and (g-i) MG-15.

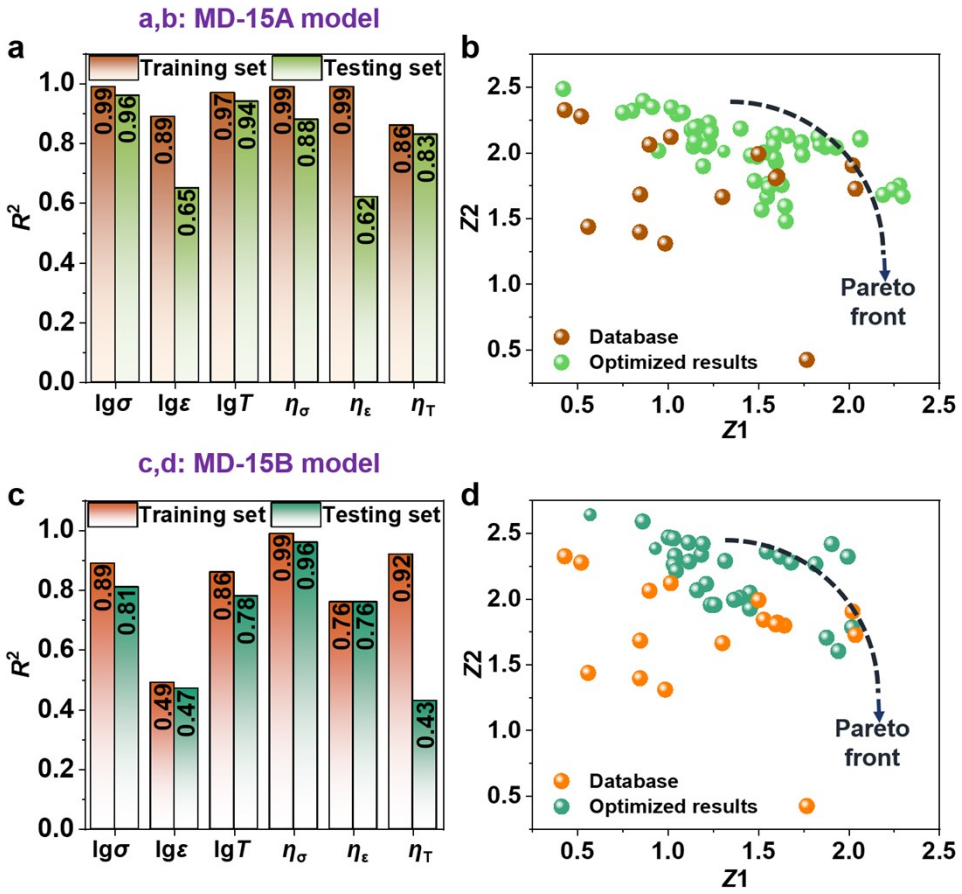

Fig. S18. Accuracy and multi-objective optimization results of MD-15A and MD-15B models. Single-objective model establishment: (a) R^2 values of MD-15A, (c) R^2 values of MD-15B. The comprehensive performance index of mechanical and self-healing properties within the dataset, along with the Pareto front based on (b) MD-15A, (d) MD-15B.

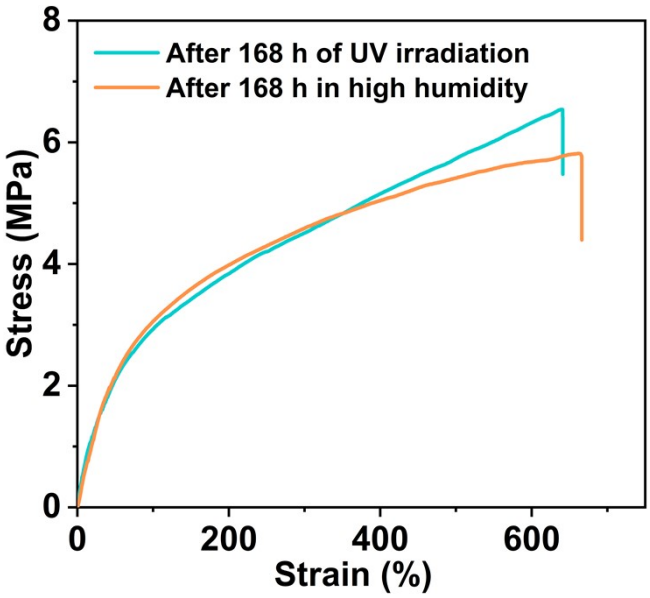

Fig. S19. Stress-strain curves of P20B after 168 hours under UV irradiation or in a high-humidity environment.

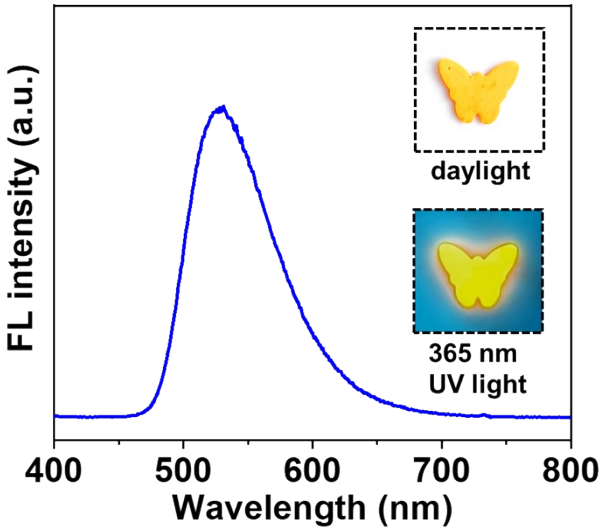

Fig. S20. Fluorescence spectroscopy (λ_{exc} = 365 nm) of P20B film (Inset: Photographs of P20B film under daylight and 365 nm UV illumination).

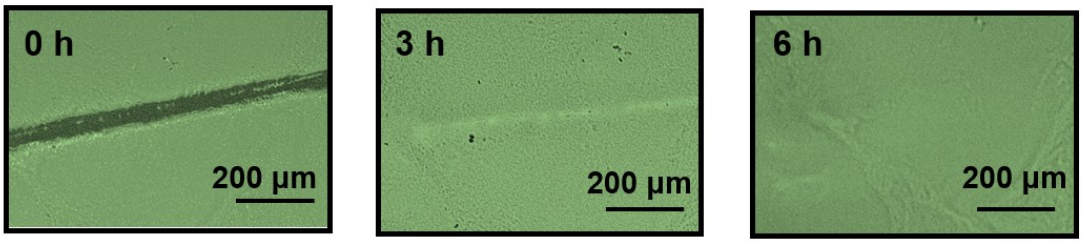

Fig. S21. Optical microscope images of scratched P20B-coated sample surface during the self-healing process at 60 ℃.

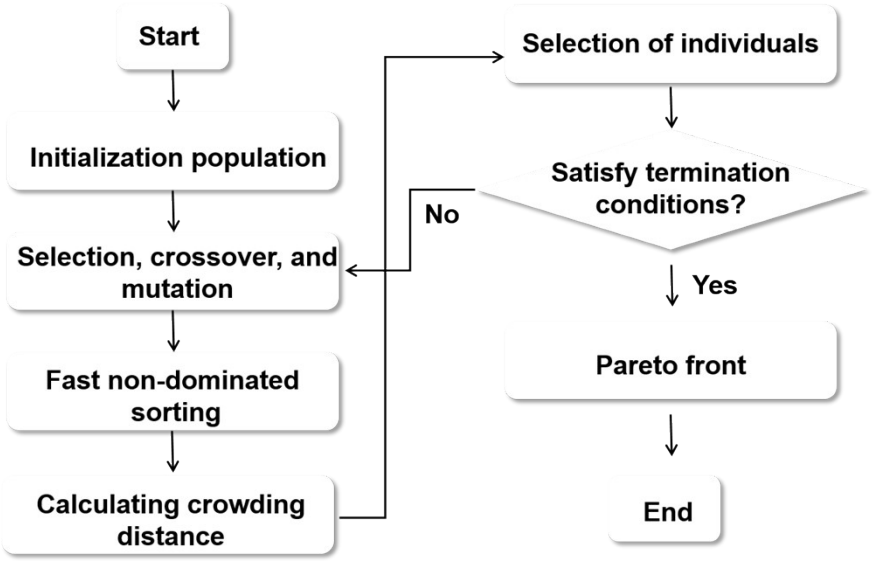

Fig. S22. The primary process of the NSGA-III algorithm.

Table S1. Machine learning training dataset for MR-9: Feature and target variable.

Entry	Samples	[PTMEG]/[IPDI]/ [HEDS]/[NIAM]	σ (MPa)	ε (%)	T (MJ m^{-3})	η_σ (%)	η_ε (%)	η_T (%)
1	P1	0.270/0.550/0.046/0.138	3.03±0.09	787.12±62.87	20.40±1.46	91.8	58.5	49.0
2	P2	0.230/0.550/0.168/0.056	2.31±0.16	946.69±171.80	18.99±4.48	91.3	68.4	60.2
3	P3	0.280/0.520/0.049/0.147	2.79±0.21	998.79±162.46	23.85±3.64	90.7	57.3	47.6
4	P4	0.260/0.520/0.108/0.108	0.29±0.02	588.21±50.15	0.81±0.08	75.9	58.0	45.7
5	P5	0.290/0.500/0/0.210	0.35±0.02	320.27±1.77	0.54±0.09	65.7	71.7	51.9
6	P6	0.270/0.500/0.058/0.173	1.19±0.09	708.45±38.15	5.82±0.24	74.8	51.8	42.1
7	P7	0.210/0.500/0.290/0	1.18±0.04	1410.39±111.72	13.46±0.72	87.3	72.6	62.2
8	P8	0.300/0.470/0/0.226	0.54±0.08	416.67±18.64	0.91±0.15	98.2	33.1	37.4
9	P9	0.220/0.470/0.306/0	0.11±0.01	1208.94±81.94	0.50±0.10	90.9	77.5	70.0

Table S2. Machine learning training dataset for MR-12: Feature and target variable.

Entry	Samples	[PTMEG]/[IPDI]/ [HEDS]/[NIAM]	σ (MPa)	ε (%)	T (MJ m^{-3})	η_σ (%)	η_ε (%)	η_T (%)
1	P1	0.270/0.550/0.046/0.138	3.03±0.09	787.12±62.87	20.40±1.46	91.8	58.5	49.0
2	P2	0.230/0.550/0.168/0.056	2.31±0.16	946.69±171.80	18.99±4.48	91.3	68.4	60.2
3	P3	0.280/0.520/0.049/0.147	2.79±0.21	998.79±162.46	23.85±3.64	90.7	57.3	47.6
4	P4	0.260/0.520/0.108/0.108	0.29±0.02	588.21±50.15	0.81±0.08	75.9	58.0	45.7
5	P5	0.290/0.500/0/0.210	0.35±0.02	320.27±1.77	0.54±0.09	65.7	71.7	51.9
6	P6	0.270/0.500/0.058/0.173	1.19±0.09	708.45±38.15	5.82±0.24	74.8	51.8	42.1
7	P7	0.210/0.500/0.290/0	1.18±0.04	1410.39±111.72	13.46±0.72	87.3	72.6	62.2
8	P8	0.300/0.470/0/0.226	0.54±0.08	416.67±18.64	0.91±0.15	98.2	33.1	37.4
9	P9	0.220/0.470/0.306/0	0.11±0.01	1208.94±81.94	0.50±0.10	90.9	77.5	70.0

10	P10	0.300/0.520/0/0.176	0.41±0.02	792.41±3.29	1.33±0.13	82.9	73.2	69.2
11	P11	0.220/0.520/0.256/0	0.92±0.01	910.67±128.55	6.62±1.04	93.5	76.0	68.4
12	P12	0.240/0.470/0.215/0.072	0.51±0.05	1602.34±70.60	3.03±0.48	86.3	52.6	47.2

*Note: The yellow-highlighted entries represent newly added sample formulations and corresponding properties compared to **Table S1**.

Table S3. Machine learning training dataset for MD-9A: Feature and target variable.

Entry	Samples	[PTMEG]/[IPDI]/ [HEDS]/[NIAM]	$\Phi 1$	$\Phi 2$	$\Phi 3$	σ (MPa)	ε (%)	T (MJ m^{-3})	η_σ (%)	η_ε (%)	η_T (%)
1	P3	0.280/0.520/0.049/0.147	1.10	0.25	0.39	2.79±0.21	998.79±162.46	23.85±3.64	90.7	57.3	47.6
2	P4	0.260/0.520/0.108/0.108	1.10	0.50	0.35	0.29±0.02	588.21±50.15	0.81±0.08	75.9	58.0	45.7
3	P13	0.240/0.520/0.177/0.059	1.10	0.75	0.32	0.28±0.02	1154.65±128.52	1.76±0.11	89.3	76.3	75.6
4	P6	0.270/0.500/0.058/0.173	1.00	0.25	0.37	1.19±0.09	708.45±38.15	5.82±0.24	74.8	51.8	42.1
5	P14	0.250/0.500/0.125/0.125	1.00	0.50	0.33	2.83±0.41	960.81±65.60	22.09±2.25	86.6	46.0	69.0
6	P15	0.230/0.500/0.203/0.068	1.00	0.75	0.30	1.83±0.05	407.02±42.49	6.08±0.88	98.4	51.5	66.0
7	P16	0.280/0.470/0.062/0.185	0.90	0.25	0.39	0.79±0.06	739.49±83.25	2.38±0.22	79.8	48.3	40.3
8	P17	0.260/0.470/0.133/0.133	0.90	0.50	0.35	0.97±0.05	2093.48±109.96	5.71±0.36	96.9	20.8	62.7
9	P12	0.240/0.470/0.215/0.072	0.90	0.75	0.32	0.51±0.05	1602.34±70.60	3.03±0.48	86.3	52.6	47.2

Table S4. Machine learning training dataset for MD-9B: Feature and target variable.

Entry	Samples	[PTMEG]/[IPDI]/ [HEDS]/[NIAM]	$\Phi 1$	$\Phi 2$	$\Phi 3$	σ (MPa)	ε (%)	T (MJ m^{-3})	η_σ (%)	η_ε (%)	η_T (%)
1	P1	0.270/0.550/0.046/0.138	1.20	0.25	0.37	3.03±0.09	787.12±62.87	20.40±1.46	91.8	58.5	49.0
2	P18	0.250/0.550/0.102/0.102	1.20	0.50	0.33	2.72±0.39	1194.64±38.58	27.92±5.39	72.1	28.0	19.2
3	P2	0.230/0.550/0.168/0.056	1.2	0.75	0.30	2.31±0.16	946.69±171.80	18.99±4.48	91.3	68.4	60.2
4	P6	0.270/0.500/0.058/0.173	1.00	0.25	0.37	1.19±0.09	708.45±38.15	5.82±0.24	74.8	51.8	42.1
5	P14	0.250/0.500/0.125/0.125	1.00	0.50	0.33	2.83±0.41	960.81±65.60	22.09±2.25	86.6	46.0	69.0
6	P15	0.230/0.500/0.203/0.068	1.00	0.75	0.30	1.83±0.05	407.02±42.49	6.08±0.88	98.4	51.5	66.0
7	P19	0.270/0.440/0.071/0.214	0.80	0.25	0.37	0.20±0.03	514.65±36.58	0.51±0.13	95.0	89.2	80.4
8	P20	0.250/0.440/0.153/0.153	0.80	0.50	0.33	0.30±0.02	911.52±26.33	1.15±0.10	93.3	38.5	43.5
9	P21	0.230/0.440/0.244/0.081	0.80	0.75	0.30	0.065±0.004	634.19±12.31	0.17±0.02	87.7	99.9	82.4

Table S5. Machine learning training dataset for MD-15: Feature and target variable.

Entry	Samples	[PTMEG]/[IPDI]/ [HEDS]/[NIAM]	$\Phi 1$	$\Phi 2$	$\Phi 3$	σ (MPa)	ε (%)	T (MJ m^{-3})	η_σ (%)	η_ε (%)	η_T (%)
1	P1	0.270/0.550/0.046/0.138	1.20	0.25	0.37	3.03±0.09	787.12±62.87	20.40±1.46	91.8	58.5	49.0
2	P18	0.250/0.550/0.102/0.102	1.20	0.50	0.33	2.72±0.39	1194.64±38.58	27.92±5.39	72.1	28.0	19.2
3	P2	0.230/0.550/0.168/0.056	1.20	0.75	0.30	2.31±0.16	946.69±171.80	18.99±4.48	91.3	68.4	60.2
4	P3	0.280/0.520/0.049/0.147	1.10	0.25	0.39	2.79±0.21	998.79±162.46	23.85±3.64	90.7	57.3	47.6
5	P4	0.260/0.520/0.108/0.108	1.10	0.50	0.35	0.29±0.02	588.21±50.15	0.81±0.08	75.9	58.0	45.7
6	P13	0.240/0.520/0.177/0.059	1.10	0.75	0.32	0.28±0.02	1154.65±128.52	1.76±0.11	89.3	76.3	75.6
7	P6	0.270/0.500/0.058/0.173	1.00	0.25	0.37	1.19±0.09	708.45±38.15	5.82±0.24	74.8	51.8	42.1
8	P14	0.250/0.500/0.125/0.125	1.00	0.50	0.33	2.83±0.41	960.81±65.60	22.09±2.25	86.6	46.0	69.0
9	P15	0.230/0.500/0.203/0.068	1.00	0.75	0.30	1.83±0.05	407.02±42.49	6.08±0.88	98.4	51.5	66.0

10	P16	0.280/0.470/0.062/0.185	0.90	0.25	0.39	0.79±0.06	739.49±83.25	2.38±0.22	79.8	48.3	40.3
11	P17	0.260/0.470/0.133/0.133	0.90	0.50	0.35	0.97±0.05	2093.48±109.96	5.71±0.36	96.9	20.8	62.7
12	P12	0.240/0.470/0.215/0.072	0.90	0.75	0.32	0.51±0.05	1602.34±70.60	3.03±0.48	86.3	52.6	47.2
13	P19	0.270/0.440/0.071/0.214	0.80	0.25	0.37	0.20±0.03	514.65±36.58	0.51±0.13	95.0	89.2	80.4
14	P20	0.250/0.440/0.153/0.153	0.80	0.50	0.33	0.30±0.02	911.52±26.33	1.15±0.10	93.3	38.5	43.5
15	P21	0.230/0.440/0.244/0.081	0.80	0.75	0.30	0.065±0.004	634.19±12.31	0.17±0.02	87.7	99.9	82.4

Table S6. Formulations of P15A and P15B.

Entry	Samples	[PTMEG]/[IPDI]/ [HEDS]/[NIAM]	$\Phi 1$	$\Phi 2$	$\Phi 3$
1	P15A	0.2260/0.6394/0.0041/0.1304	1.773	0.031	0.292
2	P15B	0.2007/0.5433/0.0005/0.2554	1.190	0.002	0.251

Table S7. Predicted and experimental properties of P15A and P15B.

Samples	Predicted properties						Experimental properties						Relative errors
	σ (MPa)	ε (%)	T (MJ m^{-3})	η_σ (%)	η_ε (%)	η_T (%)	σ (MPa)	ε (%)	T (MJ m^{-3})	η_σ (%)	η_ε (%)	η_T (%)	
P15A	10.65	837.94	23.87	89.84	54.92	54.63	6.06	165.04	8.32	0	0	0	σ: 31.3% ε: 31.8% T : 49.7%
P15B	10.65	837.94	23.87	85.43	62.26	67.22	2.98	20.74	0.41	0	0	0	σ: 116.4% ε: 122.0% T : 455.8%

Table S8. Machine learning training dataset for MD-20: Feature and target variable.

Entry	Samples	[PTMEG]/[IPDI]/ [HEDS]/[NIAM]	$\Phi 1$	$\Phi 2$	$\Phi 3$	σ (MPa)	ε (%)	T (MJ m^{-3})	η_σ (%)	η_ε (%)	η_T (%)
1	P1	0.270/0.550/0.046/0.138	1.20	0.25	0.37	3.03±0.09	787.12±62.87	20.40±1.46	91.8	58.5	49.0
2	P18	0.250/0.550/0.102/0.102	1.20	0.50	0.33	2.72±0.39	1194.64±38.58	27.92±5.39	72.1	28.0	19.2
3	P2	0.230/0.550/0.168/0.056	1.20	0.75	0.30	2.31±0.16	946.69±171.80	18.99±4.48	91.3	68.4	60.2
4	P3	0.280/0.520/0.049/0.147	1.10	0.25	0.39	2.79±0.21	998.79±162.46	23.85±3.64	90.7	57.3	47.6
5	P4	0.260/0.520/0.108/0.108	1.10	0.50	0.35	0.29±0.02	588.21±50.15	0.81±0.08	75.9	58.0	45.7
6	P13	0.240/0.520/0.177/0.059	1.10	0.75	0.32	0.28±0.02	1154.65±128.52	1.76±0.11	89.3	76.3	75.6
7	P6	0.270/0.500/0.058/0.173	1.00	0.25	0.37	1.19±0.09	708.45±38.15	5.82±0.24	74.8	51.8	42.1
8	P14	0.250/0.500/0.125/0.125	1.00	0.50	0.33	2.83±0.41	960.81±65.60	22.09±2.25	86.6	46.0	69.0
9	P15	0.230/0.500/0.203/0.068	1.00	0.75	0.30	1.83±0.05	407.02±42.49	6.08±0.88	98.4	51.5	66.0

10	P16	0.280/0.470/0.062/0.185	0.90	0.25	0.39	0.79±0.06	739.49±83.25	2.38±0.22	79.8	48.3	40.3
11	P17	0.260/0.470/0.133/0.133	0.90	0.50	0.35	0.97±0.05	2093.48±109.96	5.71±0.36	96.9	20.8	62.7
12	P12	0.240/0.470/0.215/0.072	0.90	0.75	0.32	0.51±0.05	1602.34±70.60	3.03±0.48	86.3	52.6	47.2
13	P19	0.270/0.440/0.071/0.214	0.80	0.25	0.37	0.20±0.03	514.65±36.58	0.51±0.13	95.0	89.2	80.4
14	P20	0.250/0.440/0.153/0.153	0.80	0.5	0.33	0.30±0.02	911.52±26.33	1.15±0.10	93.3	38.5	43.5
15	P21	0.230/0.440/0.244/0.081	0.80	0.75	0.30	0.065±0.004	634.19±12.31	0.17±0.02	87.7	99.9	82.4
16	P22	0.290/0.550/0/0.165	1.20	0	0.41	1.72±0.18	511.79±11.81	7.54±1.08	90.1	76.3	66.8
17	P10	0.300/0.520/0/0.176	1.10	0	0.43	0.41±0.02	792.41±3.29	1.33±0.13	82.9	73.2	69.2
18	P5	0.290/0.500/0/0.210	1.00	0	0.41	0.35±0.02	320.27±1.77	0.54±0.09	65.7	71.7	51.9
19	P8	0.300/0.470/0/0.226	0.90	0	0.43	0.54±0.08	416.67±18.64	0.91±0.15	98.2	33.1	37.4
20	P23	0.290/0.440/0/0.266	0.80	0	0.41	0.064±0.006	403.56±58.08	0.14±0.03	79.7	64.3	42.9

*Note**:** The yellow-highlighted entries represent newly added sample formulations and corresponding properties compared to **Table S5**.

Table S9. Formulations of P20A, P20B and P20C.

Entry	Samples	[PTMEG]/[IPDI]/ [HEDS]/[NIAM]	Φ1	Φ2	Φ3
1	P20A	0.2430/0.5930/0.0344/0.1296	1.457	0.210	0.321
2	P20B	0.2439/0.6067/0.0314/0.1269	1.543	0.198	0.307
3	P20C	0.2831/0.3889/0.2005/0.1275	0.637	0.611	0.395

Table S10. Predicted and experimental properties of P20A, P20B and P20C.

Samples	Predicted properties						Experimental properties						Relative errors
	σ (MPa)	ε (%)	T (MJ m^{-3})	η_σ (%)	η_ε (%)	η_T (%)	σ (MPa)	ε (%)	T (MJ m^{-3})	η_σ (%)	η_ε (%)	η_T (%)	
P20A	5.98	867.77	26.09	89.8	55.1	55.2	5.82	846.86	38.70	85.6	61.2	48.6	σ : 1.5% ε : 0.4% T :10.8% η_σ : 5.0% η_ε : 10.0% η_T : 13.6%
P20B	6.54	867.77	25.60	89.7	55.1	58.9	7.16	704.96	33.43	88.1	64.6	60.3	σ : 4.6% ε : 3.2% T : 7.6% η_σ : 1.8% η_ε : 14.7% η_T : 2.3%

P20C	0.13	867.77	0.58	91.5	61.2	56.2	0.15	836.34	0.50	93.3	67.7	78.0	σ : 7.5% ε : 0.5% T : 21.4% η_{σ} : 1.9% η_{ε} : 9.6% η_{T} : 27.9%

Table S11. Predicted and experimental comprehensive performance indicators of P20A, P20B, and P20C.

Samples	Predicted properties		Experimental properties		Relative errors
	*Z*1	*Z*2	*Z*1	*Z*2	
P20A	2.53	1.84	2.68	1.75	*Z*1: 5.6% *Z*2: 5.1%
P20B	2.60	1.87	2.75	1.92	*Z*1: 5.5% *Z*2: 2.6%
P20C	0.79	1.92	0.77	2.16	*Z*1: 2.6% *Z*2: 11.1%

Table S12. Machine learning training dataset for MD-25: Feature and target variable.

Entry	Samples	[PTMEG]/[IPDI]/ [HEDS]/[NIAM]	$\Phi 1$	$\Phi 2$	$\Phi 3$	σ (MPa)	ε (%)	T (MJ m^{-3})	η_σ (%)	η_ε (%)	η_T (%)
1	P22	0.290/0.550/0/0.165	1.20	0	0.41	1.72±0.18	511.79±11.81	7.54±1.08	90.1	76.3	66.8
2	P1	0.270/0.550/0.046/0.138	1.20	0.25	0.37	3.03±0.09	787.12±62.87	20.40±1.46	91.8	58.5	49.0
3	P18	0.250/0.550/0.102/0.102	1.20	0.50	0.33	2.72±0.39	1194.64±38.58	27.92±5.39	72.1	28.0	19.2
4	P2	0.230/0.550/0.168/0.056	1.20	0.75	0.30	2.31±0.16	946.69±171.80	18.99±4.48	91.3	68.4	60.2
5	P10	0.300/0.520/0/0.176	1.10	0	0.43	0.41±0.02	792.41±3.29	1.33±0.13	82.9	73.2	69.2
6	P3	0.280/0.520/0.049/0.147	1.10	0.25	0.39	2.79±0.21	998.79±162.46	23.85±3.64	90.7	57.3	47.6
7	P4	0.260/0.520/0.108/0.108	1.10	0.50	0.35	0.29±0.02	588.21±50.15	0.81±0.08	75.9	58.0	45.7
8	P13	0.240/0.520/0.177/0.059	1.10	0.75	0.32	0.28±0.02	1154.65±128.52	1.76±0.11	89.3	76.3	75.6
9	P5	0.290/0.500/0/0.210	1.00	0	0.41	0.35±0.02	320.27±1.77	0.54±0.09	65.7	71.7	51.9

10	P6	0.270/0.500/0.058/0.173	1.00	0.25	0.37	1.19±0.09	708.45±38.15	5.82±0.24	74.8	51.8	42.1
11	P14	0.250/0.500/0.125/0.125	1.00	0.50	0.33	2.83±0.41	960.81±65.60	22.09±2.25	86.6	46.0	69.0
12	P15	0.230/0.500/0.203/0.068	1.00	0.75	0.30	1.83±0.05	407.02±42.49	6.08±0.88	98.4	51.5	66.0
13	P8	0.300/0.470/0/0.226	0.90	0	0.43	0.54±0.08	416.67±18.64	0.91±0.15	98.2	33.1	37.4
14	P16	0.280/0.470/0.062/0.185	0.90	0.25	0.39	0.79±0.06	739.49±83.25	2.38±0.22	79.8	48.3	40.3
15	P17	0.260/0.470/0.133/0.133	0.90	0.50	0.35	0.97±0.05	2093.48±109.96	5.71±0.36	96.9	20.8	62.7
16	P12	0.240/0.470/0.215/0.072	0.90	0.75	0.32	0.51±0.05	1602.34±70.60	3.03±0.48	86.3	52.6	47.2
17	P23	0.290/0.440/0/0.266	0.80	0	0.41	0.064±0.006	403.56±58.08	0.14±0.03	79.7	64.3	42.9
18	P19	0.270/0.440/0.071/0.214	0.80	0.25	0.37	0.20±0.03	514.65±36.58	0.51±0.13	95.0	89.2	80.4
19	P20	0.250/0.440/0.153/0.153	0.80	0.50	0.33	0.30±0.02	911.52±26.33	1.15±0.10	93.3	38.5	43.5
20	P21	0.230/0.440/0.244/0.081	0.80	0.75	0.30	0.065±0.0	634.19±12.31	0.17±0.02	87.7	99.9	82.4

						04					
21	P15A	0.2260/0.6394/0.0041/0.1304	1.773	0.031	0.292	6.06±0.24	165.03±29.71	8.32±1.97	0	0	0
22	P15B	0.2007/0.5433/0.0005/0.2554	1.190	0.002	0.251	2.98±0.31	20.74±1.77	0.41±0.11	0	0	0
23	P20A	0.2430/0.5930/0.0344/0.1296	1.457	0.210	0.321	5.82±0.23	846.86±27.01	38.7±1.93	85.6	61.2	48.6
24	P20B	0.2439/0.6067/0.0314/0.1269	1.543	0.198	0.307	7.16±0.22	704.96±66.39	33.43±3.68	88.1	64.6	60.3
25	P20C	0.2831/0.3889/0.2005/0.1275	0.637	0.611	0.395	0.15±0.01 5	836.34±120.86	0.50±0.08	93.3	67.7	78.0

Note: The yellow-highlighted entries represent newly added sample formulations and corresponding properties compared to **Table S8**.

Table S13. Machine learning training dataset for MG-15: Feature and target variable.

Entry	Samples	[PTMEG]/[HMDI]/[BP]/[PDM]	$\Phi 1$	$\Phi 2$	$\Phi 3$	σ (MPa)	ε (%)	T (MJ m^{-3})	η_σ (%)	η_ε (%)	η_T (%)
1	PG1	0.270/0.550/0.046/0.138	1.20	0.25	0.37	0.41±0.02	3237.19±164.58	6.42±0.97	92.7	59.7	72.0
2	PG2	0.250/0.550/0.102/0.102	1.20	0.50	0.33	7.46±0.38	1397.75±85.81	49.91±4.41	28.8	40.6	17.1
3	PG3	0.230/0.550/0.168/0.056	1.20	0.75	0.30	0.48±0.03	2954.21±63.36	4.80±0.85	100.0	91.5	83.8
4	PG4	0.280/0.520/0.049/0.147	1.10	0.25	0.39	0.13±0.01	1693.54±272.93	0.69±0.07	100.0	50.0	66.7
5	PG5	0.260/0.520/0.108/0.108	1.10	0.50	0.35	0.22±0.02	1728.53±141.20	1.47±0.08	95.5	34.8	52.4
6	PG6	0.240/0.520/0.177/0.059	1.10	0.75	0.32	4.44±0.38	2326.25±53.83	58.75±3.66	95.3	72.3	69.3
7	PG7	0.270/0.500/0.058/0.173	1.00	0.25	0.37	0.13±0.00	2686.07±261.86	0.86±0.04	100.0	26.7	57.0
8	PG8	0.250/0.500/0.125/0.125	1.00	0.50	0.33	0.25±0.01	3037.39±70.60	2.38±0.34	96.0	60.7	76.5
9	PG9	0.230/0.500/0.203/0.068	1.00	0.75	0.30	0.88±0.05	4706.15±107.49	16.75±3.00	96.6	98.7	100.0
10	PG10	0.280/0.470/0.062/0.185	0.90	0.25	0.39	0.13±0.01	1071.45±96.84	0.48±0.07	84.6	59.3	77.1
11	PG11	0.260/0.470/0.133/0.133	0.90	0.50	0.35	0.41±0.01	3942.87±117.47	6.74±0.97	100.0	96.8	86.1

12	PG12	0.240/0.470/0.215/0.072	0.90	0.75	0.32	2.93±0.05	2286.62±176.31	35.77±6.98	83.3	78.9	66.2
13	PG13	0.270/0.440/0.071/0.214	0.80	0.25	0.37	0.11±0.01	2186.69±219.61	0.71±0.09	90.9	39.8	57.8
14	PG14	0.250/0.440/0.153/0.153	0.80	0.50	0.33	0.13±0.01	1746.53±196.33	0.76±0.05	84.6	27.2	32.9
15	PG15	0.230/0.440/0.244/0.081	0.80	0.75	0.30	0.39±0.02	3194.95±237.98	4.70±0.31	100.0	88.5	98.3

Table S14. Formulations of PG15A, PG15B and PG15C.

Entry	Samples	[PTMEG]/[HMDI]/ [BP]/[PDM]	$\Phi 1$	$\Phi 2$	$\Phi 3$
1	PG15A	0.2569/0.5284/0.1505/0.0641	1.120	0.701	0.346
2	PG15B	0.2567/0.5137/0.1631/0.0664	1.056	0.711	0.345
3	PG15C	0.2557/0.6788/0.0013/0.0642	2.113	0.021	0.343

Table S15. Predicted and experimental properties of PG15A, PG15B and PG15C.

Samples	Predicted properties						Experimental properties						Relative errors
	σ (MPa)	ε (%)	T (MJ m^{-3})	η_σ (%)	η_ε (%)	η_T (%)	σ (MPa)	ε (%)	T (MJ m^{-3})	η_σ (%)	η_ε (%)	η_T (%)	
PG15A	4.33	2894.40	33.87	100.0	97.9	93.0	3.91	2482.09	61.41	89.0	81.8	82.6	σ : 7.5% ε : 1.9% T :14.5% η_σ :12.4% η_ε :14.9% η_T : 14.8%
PG15B	4.33	2994.34	33.87	100.0	88.9	96.4	3.56	2639.64	67.38	91.0	90.1	80.7	σ : 15.4% ε : 1.6% T : 16.3% η_σ : 9.9% η_ε : 1.3% η_T : 19.5%

PG15C	6.33	2714.48	41.70	97.0	71.4	83.8	10.83	310.99	19.95	0	0	0	σ : 22.5% ε : 37.7% T : 24.6% η_{σ} : - η_{ε} : - η_{T} : -

Table S16. Predicted and experimental comprehensive performance indicators of PG15A, PG15B, and PG15C.

Samples	Predicted properties		Experimental properties		Relative errors
	*Z*1	*Z*2	*Z*1	*Z*2	
PG15A	1.82	2.47	1.98	2.20	*Z*1: 8.1% *Z*2: 12.3%
PG15B	1.83	2.43	2.02	2.25	*Z*1: 9.4% *Z*2: 8.0%
PG15C	2.00	2.19	1.78	0	*Z*1: 12.4% *Z*2: -

Table S17. Hyperparameter search ranges for GBR.

Algorithm	Hyperparameter search ranges
GBR	random_state: (0, 20, 1), n_estimators: (1, 200, 5), max_depth: (1, 20, 1),

*Note: If the model accuracy is poor, fine-tuning of max_features will be adjusted.

References

[1] N. Srinivas and K. Deb, *Evol. Comput.*, 1994, **2**, 221-248.

[2] K. Deb, A. Pratap, S. Agarwal and T. Meyarivan, *IEEE T. Evolut. Comput.*, 2002, **6**, 182-197.

[3] K. Deb and H. Jain, *IEEE T. Evolut. Comput.*, 2014, **18**, 577-601.